EFFECT OF THE INCLINATION ANGLE OF FINNED CYLINDER OVER A BFS ON THE MHD BEHAVIOR IN THE PRESENCE OF A NANOFLUID

Djamila Derbal, Mohamed Bouzit, Fayçal Bouzit*

University of Science and Technology of Oran, Faculty of Mechanical Engineering, Laboratoire des sciences et ingenerie maritime LSIM, Mohamed Boudiaf, El Mnaouar, BP 1505, Bir El Djir 31000, Oran, Algeria

Abstract

The present numerical study is based on the forced magnetohydrodynamic (MHD) convection of a ferrofluid through a backward facing step (BFS). A cylinder with two fixed fins and fixed dimensions is implanted inside fluid. The dimensionless governing equations have been solved using the multigrid finite element method. Several parameters were considered, such as the Hartmann number $0 \leq Ha \leq 100$, the magnetic field inclination angle $0° \leq \gamma \leq 90°$, the Reynolds number $10 \leq Re \leq 200$, the nanoparticle volume fraction $0\% \leq \varphi \leq 10\%$, and the fins inclination angle $0° \leq a \leq 180°$. The results have shown that the presence of the fins improves the heat transfer, especially at the position $a = 90°$ where the Nuave number increases with a ratio of 113% for $Re = 200$.

Introduction

The sudden expansion of geometry in conduit makes the reason for the existence of a flows separation and reattachment, where it was a prime factor in determining the structure of the flow and significantly affects the mechanism of heat transfer. Thus, the backward-facing step geometry plays a very important role in engineering applications such as combustion chambers, airplanes, gas turbine engines, electronic devices, heat exchangers, around buildings, and many others of a kind. So it received much attention, where many studies have focused on the separation and reattachment of the flow backward-facing step.

Corresponding author: Djamila Derbal, djamila.derbal@univ-usto.dz

Erturk [1] presented Numerical solutions of 2-Dlaminar steady incompressible flow at high Reynolds numbers. In three dimensions, *Lan et al.* [2] provided a numerical study of laminar forced convection flow in a rectangular duct using a K-ε-ζ-f turbulence model. At low Reynolds number, *Iwai et al.* [3] have investigated the effects of the duct aspect ratio, and the maximum Nusselt number did not appear on the centerline but near the two side walls in every case. At different Richardson number, *Star ("Kelbij") et al.* [4] proposed a POD-Galerkin reduced order modeling strategy for (RANS) simulation that is extended for low-Prandtl number flow. It shows that buoyancy has large influence on the flow and heat transfer.

We add that for a better forecast of the flow structure, the knowledge of the characteristics of the fluids as well as the identification of the consequences of rheo-fluidification is interesting. *Kahin et al.* [5] proposed a numerical simulation compared to the experimental studies, where the stabilizing effect of the shear-thinning character of the fluid is highlighted. For depicting the power law relation between viscosity and shear rate and Newtonian materials, *Mahmood et al.* [6], with a finite element method, devoted to analyzing the flow of the power law fluid representing the features of shear thinning, thickening, and Newtonian materials. In turbulent flows, their control can be achieved by an external force, stable or unstable, representing a fundamental and practical interest [7]. For *Benard et al.* [8] and *Li et al.* [9], these experimental studies were of interest for researching the influence of periodic perturbations, frequency, and amplitude imposed on the vortex´s development of a separated shear layer, formed downstream of a (BFS). In the low Reynolds number, *Koide et al.* [10] tried to improve heat transfer. They proposed a numerical simulation compared with experimental data to investigate the effects of operating parameters of a periodic disturbance introduced in the flow behind a backward facing step (BFS) on a reattaching flow. On the transient flow regime, *Tihon et al.* [11] proposed an experimental study of a (BFS) to investigate the organization of the flow near the wall by mapping the fluctuating shear rate of the wall downstream of the stage, as well as the effect of inlet flow pulses on the overall flow structure.

Heat transfer is the main focus of many studies, and for each study, there is an interest in improving it according to the needs of the process. One recent technique that is used to improve heat transfer in fluids by convection between the fluid and the surface is the injection of nanoparticles into these fluids. More recent research has shown the effectiveness of their presence in the base fluids. Adding nanoparticles, *Selimefendigil et al.* [12] explored the effects of its volume fraction, oscillation, and frequency, imposed at the inlet and Reynolds number on the fluid flow and heat transfer characteristics. It is observed that heat transfer is enhanced by increasing the oscillation frequency, nanoparticle volume fraction, and Reynolds number.

Another aim of the present study is to obtain nonlinear dynamic models. *Hilo et al.* [13] investigated the forced convective heat transfer and friction factor of nanofluids flow over a backward-facing step and found that the heat transfer rate increased as the volume concentration of nanoparticles increased. *Togun* [14] presented a numerical study of heat transfer to turbulent and laminar of nanofluid flow over a backward-facing step to clearly observe the expansion rate's effect, considering several governing parameters. Using different vortex generators at different angles of inclination, *Ahmed et al.* [15] have studied a forced convection heat transfer of a laminar fluid flow on a micro-scale (BFS). Their result shows that the heat transfer is enhanced with a slight increase in the pressure drop in the case of rectangular wing VG at an attack angle of 60° and Reynolds number

of 180. Numerical simulations are performed for a laminar flow of an electrically conductive viscous incompressible fluid in a backward-facing step under the action of a magnetic field for a particular Reynolds number [16]. The heat transfer is discussed for a range of Prandtl number value, *Kumar and Dhiman* [17] investigated the increasing laminar forced convection characteristics of the backward-facing step flow in a two-dimensional channel. They treated the effect of cylinder position on flux and heat transfer at a Pranldt number and for different values of Re, an enhancement in the Nusselt number using a circular cylinder compared to the without cylinder case.

Hussain et al. [18] were used the Galerkin finite element method to simulate the forced convective flow of Ferrofluid inside a (BFS) including a rotating cylinder with fixed diameter, wide ranges of the governing parameters were considered. *Mohammed* [19] studied numerically the effects of four various types of blockage shapes transient laminar mixed convective nanofluid flow over a horizontal BFS placed in a duct. By using a microscale (BFS) placed in a horizontal duct, *Kherbeet et al.* [20] investigated experimentally and numerically a laminar forced convective flow, utilizing nanofluid with two types of nanoparticles. They found that Nusselt improves in the presence of one nanofluid compared to another as well as its increase. The analysis made by *Lv and Hu* [21] on several parameters found that the flow characteristics are quantitatively studied using PIV in two-dimensional backward step flow and that by changing the Reynolds number and weight fraction of the nanofluid, the mass and momentum transfer in nanofluid is enhanced, resulting in heat transfer enhancement. *Amiri et al.* [22] presented an experimental study on thermo-physical properties of EGGNP and a numerical one on the convective heat transfer over a (BFS). According to their results, a higher weight concentration of nanofluid implies a higher rate of heat transfer on a backward facing stage. *Niemann et al.* [23] studied the impact of buoyancy effects on the velocity field and on turbulent heat transfer in the mixed regime by comparing two simulations, one with the buoyancy term removed from the equations and the other with a Richardson number of 0.338. On an inclined step in an inclined duct, *Atashafrooz* [24] presented the influence of buoyancy force on nanofluid flow in mixed MHD convection and entropy generation where the interaction of several parameters is studied, in an abruptly contracting duct [25], in a trapezoidal recess [26], and in three-dimensional forced convection [27], radiative heat transfer plays an important role in thermal behavior, so considering the interactions between the different radiative and convective (or conductive) heat transfer mechanisms can improve simulation precision [28-33].

To see the effect of fins on heat transfer, *Boruah et al.* [35] tested the thermo-hydraulic characteristics and entropy generation for mixed convective flow through a (BFS) channel with baffle with variable geometries. The result showed that in a staggered arrangement, the elliptical baffles in (BFS) channel is an optimum design choice from the thermo-hydraulic performance and entropy generation perspective. However, heat transfer and fluid flow characteristics over a backward or forward facing step in a channel with the insertion of obstacles have received less attention in the literature [36]. *Selimefendigil and Öztop* [37] examined numerically a laminar pulsating flow, a forced convective heat transfer in channel over a backward facing step having a baffle on the top wall. The effects of various pertinent parameters were studied compared to steady flow with no fin case, adding a fin is not advantageous for heat transfer enhancement in pulsating flow. With a corrugated bottom wall, *Selimefendigil et al.* [38] numerically studied laminar forced convection of pulsating nanofluid flow over a (BES). They treated

the effect of the length and height of the surface corrugation at the bottom wall, and wide ranges of the governing parameters were considered. The presence of additional surface corrugation results in less effective heat transfer. *Selimefendigil et al.* [39] a finite element method was used, numerically they presented the effect of inclination angles of magnetic field on laminar forced convection of nanofluid flow over (BFS) and wide ranges of the governing parameters were considered. With a different baffle configurations distance, variable number and arrangement, *Boruah et al.* [40] presented numerically a two-dimensional, steady, laminar, incompressible and mixed convective flow of non-Newtonian fluid through (BFS) channel. The output is useful in designing a thermodynamic system that can provide maximum heat transfer with minimum irreversibility. By adding the effect of the position of the baffle on the upper wall and the type and diameter of the nanoparticles, *Mohammed* [41] has simulated numerically two-dimensional laminar and turbulent mixed convection flows using nanofluid over backward facing step. The effects of baffle distance heights and baffle locations on fluid flow and heat transfer characteristics are significant, while the effects of baffle widths and numbers are slightly insignificant. *Heshmati and Mohammed* [42] add the effect of four-geometry baffles at different inclinations and positions, and different parameters were considered. *Mokhefi et al.* [43-46] performed numerical simulations to study the laminar flow behavior of anchor-induced nanofluids in stirred vessels using the single-phase nanofluid model, where heat transfer is significant with the progressive addition of alumina nanoparticles with an increase in stirring power consumption.

The comparative analysis of previous work on MHD, BFS, and nanofluids has shown that no work on thermo-magnetohydrodynamic behavior has been performed by installing adiabatic fins. Furthermore, it seems clear that no work has been carried out to determine the best position of these fins leading to the best heat transfer.

Hence, the present study aims to provide a numerical simulation on the forced laminar convective flow, in the presence of Fe_3O_4 and H_2O ferrofluids, inside a backward-facing geometry and using a single phase nanofluid model. This geometry contains two fins installed on a fixed cylinder under the influence of an inclined magnetic field. The effect of the position of these fins has been highlighted on the thermal and hydrodynamic structures for different values of different control parameters. The finite element method was used to solve the equations that govern the flow under study.

Geometric description

The physical situation studies the forced convection of a two-dimensional, laminar, incompressible and Newtonian flow of a ferrofluid through the backward step, a fixed cylinder of diameter D equipped with two fins of a length less than or equal to the radius of this cylinder. The latter is placed in the center at (4H, H), is shown schematically in Fig.1. The step height is taken as H, halfway up the canal. The expansion ratio is set equal to 2 and the external magnetic field is imposed at an angle γ. The effects of viscous dissipation and Joule heating are not considered while modeling the energy equation. The induced magnetic field is supposed to be negligible. At the inlet, the ferrofluid is considered cold at a temperature Tc, while the lower wall downstream of the step is maintained at a high temperature T_h and the rest walls are kept thermally insulated. Thermophysical properties of water and Iron Oxide are presented in Table 1. The physical configuration subjected to the boundary conditions are demonstrated in Fig.1.
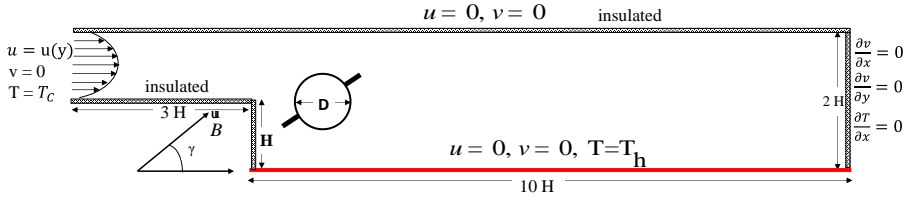
Fig. 1. Diagram of the physical configuration with the boundary conditions.

Table 1. Thermophysical properties of Water (H_2O) and Iron Oxide nanoparticles.

Physical properties	Water (H_2O)	Nanoparticles (Fe_3O_4)
Density [kgm^{-3}]	997.1	5200.0
Specific heat [$Jkg^{-1}K^{-1}$]	4179	670.00
Thermal conductivity [$Wm^{-1}K^{-1}$]	0.613	6.0000
Thermal expansion [K^{-1}] ($\times 10^{-5}$)	0.613	1.1800
Electrical conductivity [Sm^{-1}]	0.050	25000

Mathematical model

Gouverninig equations

The Laminar forced convection flow of a nanofluid over a backward facing step geometry that contains a fixed finned cylinder is governed by the partial differential equations that express the conservation of mass, momentum, and energy:

$$\frac{\partial u}{\partial x} + \frac{\partial v}{\partial y} = 0 \qquad\qquad 1$$

$$\rho_{ff}\left(u\frac{\partial u}{\partial x} + v\frac{\partial u}{\partial y}\right) = \left(-\frac{\partial p}{\partial x} + \mu_{ff}\left(\frac{\partial^2 u}{\partial x^2} + \frac{\partial^2 u}{\partial y^2}\right) + \sigma_{np}B_0^2(vsin\gamma cos\gamma - usin^2\gamma)\right) \qquad 2$$

$$\rho_{ff}\left(u\frac{\partial v}{\partial x} + v\frac{\partial v}{\partial y}\right) = \left(-\frac{\partial p}{\partial y} + \mu_{ff}\left(\frac{\partial^2 v}{\partial x^2} + \frac{\partial^2 v}{\partial y^2}\right) + \sigma_{ff}B_0^2(usin\gamma cos\gamma - vcos^2\gamma)\right) \qquad 3$$

$$\rho_{ff}\left(u\frac{\partial v}{\partial x} + v\frac{\partial v}{\partial y}\right) = \left(-\frac{\partial p}{\partial y} + \mu_{ff}\left(\frac{\partial^2 v}{\partial x^2} + \frac{\partial^2 v}{\partial y^2}\right) + \sigma_{ff}B_0^2(usin\gamma cos\gamma - vcos^2\gamma)\right) \qquad 4$$

The following equation presents the stream function.

$$\frac{\partial \Psi}{\partial x} = -v \text{ , and } \frac{\partial \Psi}{\partial y} = u \qquad\qquad 5$$

Boundary conditions

The boundary conditions imposed for the numerical computation of the studied field can be expressed as follows:

At the channel inlet: A parabolic velocity profile in the horizontal direction and a uniform, cold temperature:

u = u(y), v=0 and T=T_c   *6*

At the downstream bottom wall: The no-slip velocity boundary conditions and a uniform hot temperature:

u=v=0, T=T_h   *7*

At the channel outlet: The gradient of velocity and temperature variables in the x-direction (normal direction coincide with x axis) are:

$\frac{\partial u}{\partial n} = \frac{\partial v}{\partial n} = 0$ *and* $\frac{\partial T}{\partial n} = 0$ *8*

Except the bottom wall, the adiabatic conditions for the temperature and no-slip boundary conditions for velocity are prescribed on the channel walls:

$u = v = 0, \frac{\partial T}{\partial n} = 0$ *9*

On the border of the cylinder, the adiabatic conditions for the temperature and the following velocity are imposed:

$u = v = 0, \frac{\partial T}{\partial n} = 0$ *10*

Dimensionless governing equations
To transform the system of partial differential equations into dimensionless form, the following variables are used presented in Table 2.

Table 2. The variables are used to transform the system of partial differential equations in to dimensionless form.

$X = \frac{x}{H}, Y = \frac{y}{H}$	$U = \frac{u}{\bar{u}}, V = \frac{v}{\bar{u}}$	$P = \frac{p}{\rho_{ff}\bar{u}^2}, \tau = \frac{t\bar{u}}{H}$
$\theta = \frac{T - T_c}{T_h - T_c}$	$Pr = \frac{\nu_f}{\alpha_f}, Re = \frac{H\bar{u}}{\nu_f}$	$Ha = B_0 H \sqrt{\frac{\sigma_{ff}}{\mu_{ff}}}$

The dimensionless equations governing are reduced as follows:

$$\frac{\partial U}{\partial X} + \frac{\partial V}{\partial Y} = 0$$ *11*

$$U\frac{\partial U}{\partial X} + V\frac{\partial U}{\partial Y} = -\frac{\partial P}{\partial X} + \frac{1}{Re}\frac{\mu_{ff}}{\rho_{ff}\nu_f}\left(\frac{\partial^2 U}{\partial X^2} + \frac{\partial^2 U}{\partial Y^2}\right) + \frac{\rho_f}{\rho_{ff}}\frac{\sigma_{ff}}{\sigma_f}\frac{Ha^2}{Re}(V sin\gamma cos\gamma -$$

$$U sin^2\gamma)$$ *12*

$$U\frac{\partial V}{\partial X} + V\frac{\partial V}{\partial Y} = -\frac{\partial P}{\partial Y} + \frac{1}{Re}\frac{\mu_{ff}}{\rho_{ff}\,\nu_f}\left(\frac{\partial^2 V}{\partial X^2} + \frac{\partial^2 V}{\partial Y^2}\right) + \frac{\rho_f}{\rho_{ff}}\frac{\sigma_{ff}}{\sigma_f}\frac{Ha^2}{Re}(Usin\gamma cos\gamma -$$

$$Vcos^2\gamma)\tag{13}$$

$$U\frac{\partial \theta}{\partial X} + V\frac{\partial \theta}{\partial Y} = \frac{1}{Re\,Pr}\frac{\alpha_{ff}}{\alpha_f}\left(\frac{\partial^2 \theta}{\partial X^2} + \frac{\partial^2 \theta}{\partial Y^2}\right)\tag{14}$$

The dimensionless equations stream function is given as follows:

$$\frac{\partial \Psi}{\partial X} = -V \ and \ \frac{\partial \Psi}{\partial Y} = U\tag{15}$$

Table 3.The boundary conditions are implemented in dimensionless form.

At the channel inlet:	$U = U(y), V = 0, \theta = 0, \dfrac{\partial \Psi}{\partial Y} = 1$
At the downstream bottom wall:	$U = 0, V = 0, \theta = 1, \dfrac{\partial \Psi}{\partial Y} = 0$
At the channel outlet:	$\dfrac{\partial U}{\partial X} = \dfrac{\partial V}{\partial X} = \dfrac{\partial \theta}{\partial X} = 0, \dfrac{\partial \Psi}{\partial Y} = U_s$
On the channel walls (except the bottom wall):	$U = V = \dfrac{\partial \theta}{\partial n} = 0, \Psi = 0$
On the boundary of cylinder:	$U = V = 0, \dfrac{\partial \theta}{\partial n} = 0, \ \Psi = 0$

Table 4. The effective thermophysical properties of the nanofluid

Density:	$\rho_{ff} = (1 - \varphi)\rho_f + \varphi\rho_s,$
Thermal diffusivity:	$\alpha_{ff} = \dfrac{k_{ff}}{(\rho\,C_p)_{ff}}$
Electrical conductivity:	$\sigma_{ff} = \sigma_f\left(1 + \dfrac{3(\sigma - 1)\varphi}{(\sigma + 2) - (\sigma - 1)\varphi}\right), \ \sigma = \dfrac{\sigma_s}{\sigma_f}$
Specific heat:	$(\rho\,Cp)_{ff} = (1 - \varphi)(\rho Cp)_f + \varphi(\rho Cp)_s$
Thermal expansion coefficient:	$(\rho\beta)_{ff} = (1 - \varphi)(\rho\beta)_f + \varphi(\rho\beta)_s$
Thermal conductivity:	$\dfrac{k_{ff}}{k_f} = \dfrac{k_s + 2k_f - 2\varphi(k_f - k_p)}{k_s + 2k_f + \varphi(k_f - k_p)}$
Dynamic viscosity:	$\mu_{ff} = \dfrac{\mu_f}{(1 - \varphi)^{2.5}}$

In the dimensionless form, the implemented boundary conditions take the form illustrated in Table 3. The thermophysical properties of ferrofluid depend on the properties of the base fluid and magnetized particles. The effective Thermophysical properties of the nanofluid are considered as follows in Table 4.

The local and Nu_{ave} number

Heat transfer is mainly analyzed using the Nusselt number that measures the ratio of heat transfer rates by convection and conduction. The local, respectively the mean Nusselt number on the heated wall are calculated as follows:

$$Nu = \frac{h_{ff}.L}{k_f}$$ 16

Where h_{ff} is the coefficient of heat transfer:

$$h_{ff} = \frac{q_w}{T_h - T_c}$$ 17

Where q_w stands for heat flux on the heated wall:

$$q_w = -k_{ff} \frac{T_h - T_c}{L} \frac{\partial \theta}{\partial y}\Big|_{y=0}$$ 18

$$Nu = \frac{k_{ff}}{k_f} \frac{\partial \theta}{\partial Y}$$ 19

The Nu_{aver} number is obtained by integrating the local Nusselt along the length of the bottom wall as:

$$Nu_{ave} = \frac{1}{L_s} \int_0^{L_s} Nu \, dX$$ 20

Where L_s represent the local length of the heated part.

Code validation and grid independence test

The system of equations (11) - (14), with boundary conditions, was solved by the finite element method based on the Galerkin discretization. The adopted mesh of the computation domain is an unstructured triangular shape, as shown in Fig. 2. The criterion of convergence of the different independent variables must be less than 10^{-6}.

The independent grid study is presented in Table 5 for Nu_{ave} number and the θ_{ave} for the case $a = 90°$ at Pr = 6.2, Re =100, Ha = 20, $\gamma = 0°$, $\varphi = 0.04$, which indicates that the difference between the values of the levels of the last three grids is very small. The calculations are therefore carried out at the level of the grid having 42359 total numbers of elements.

(a)   *(b)*

Fig. 2. Mesh (a) inside the computational domain (b) zoom in the vicinity of the fin.

To verify the accuracy of these numerical results, the calculation code was validated with the numerical results of *Hussain and Ahmed* [18], who studied the forced convection of a laminar flow of a ferrofluid inside backward-facing step. We have

demonstrated the shape of the isotherms at Re = 10 and Re =200 for the values of Pr = 6.2, Ha = 25, γ = 0°, φ = 0.05 (Fig. 4). The Nusselt curve as a function of the Reynolds number is also plotted for Pr = 6.2, Ha = 25, γ = 0°, φ = 0.1. It is clear from (Fig. 3) that our numerical results are in good agreement with the results obtained by *Hussain and Ahmed* [18].

Table 5. The average number of Nusselt and Temperature for several numbers of elements

Number of elements	4826	14182	42359	88588	150225
Time	11 s	21 s	71 s	244 s	270 s
Nu_{ave}	4.70111	4.68138	4.67116	4.67493	4.67455
θ_{ave}	0.10047	0.10108	0.10140	0.10128	0.10127
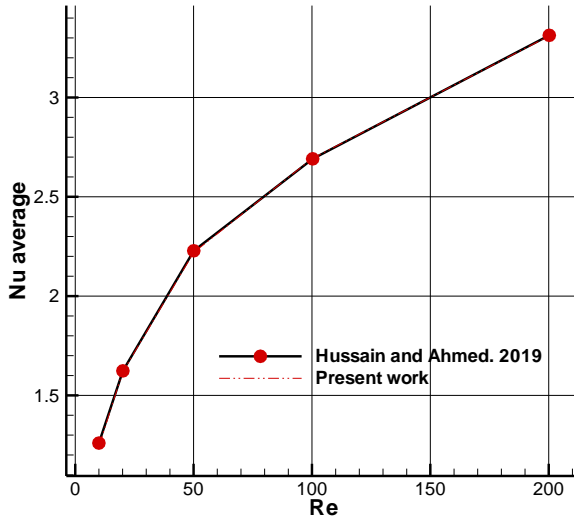
Fig. 3. Comparison of the isotherms of the present study with the reference [18] for Pr = 6.2, Ha = 25, γ = 0°, φ = 0.05.
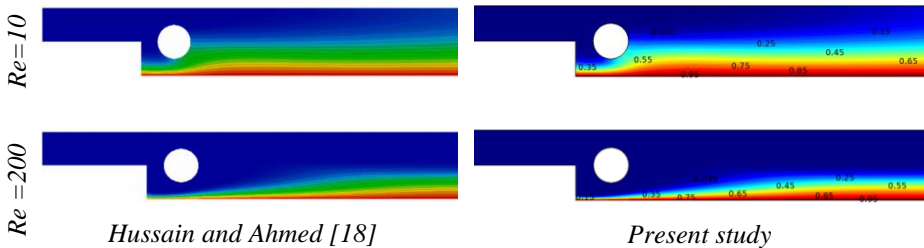
Fig. 4. Comparison of the isotherms of the present study with the reference [18] for Pr = 6.2, Ha = 25, γ = 0°, φ = 0.05.

Results and Discussion

The effects of variations in different control parameters on streamlines, isotherms and Nu_{ave} number are discussed in this section. The simulation is based on the demonstration for each value of fin angle a (0°, 30°, 60°, 90°), the effect of the number of Hartmann Ha (0, 20, 50), the angle of inclination of the magnetic field γ (0°, 60°, 90°), the Reynolds number Re (10, 100, 200), and the volume fraction of the nanoparticles φ (0%, 4%, 10%). Water is the basic fluid in the formation of the ferrofluid with $Pr = 6.2$. The results obtained are presented in Figs. 5-8, as well as the variation of the Nu_{ave} number is shown in Figs. 9-10.

Fig. 5 shows the contours of streamlines and isotherms for the variation of the Hartmann number: $Ha = 0$, $Ha=20$ and Ha = 50 at different fins inclination angles: $a=$ (0°, 30°,60°,90°) for $Pr = 6.2$, $Re = 50$, $\gamma = 0°$ et $\varphi = 4\%$. For the first two inclination angle, the fluid makes a strong flow at the inlet and at the top of the wall and weak flow at the bottom of the cylinder. This behavior took place at $Ha=0$ to decrease further until $Ha=50$. Physically this phenomenon is explained by the presence of the magnetic force that obstructs the flow of the fluid. For $a=$ (30°, 60°) at $Ha=0$ the ferrofluid flows with very important velocities around fins which will be more important at the near the upper one at $Ha = 20$, to disappear at the lower fin in the position $a= 60°$ at $Ha = 50$, remain important at the angle $a = 90°$,caused the separation of the flow around the fin and will affect the convective heat transfer at the heated wall, where the ffferrofluid concentrates and the contact with the hot wall is better. However, the isotherms begin to extend toward the top wall (adiabatic) so the thermal boundary layer (at the bottom of the heated wall) decreases. Contrary to the position $a = 90°$ where the thermal layer increases at $Ha=20$ then a good heat transfer, we note $Nu_{ave} = 3.7$ (Fig. 9 (a)) to mark an improvement at $Ha=50$, where the forced convection is better. 0

The streamlines and isotherms for different values of the fin inclination angle: $a =$ (0°,30°,60°,90°) at different angles of inclination of the magnetic field, horizontal $\gamma =0$ °, inclined magnetic field $\gamma =60°$ and the vertical magnetic field $\gamma =90°$are demonstrated in Fig. 6. All these cases are calculated at $Pr = 6.2$, $Re =100$, $Ha =20$ and $\varphi = 4\%$. For $\gamma = 0°$ and at the position $a= 0°$ the rate of fluid movement is lowest at the bottom of the cylinder, improved at the position $a=30°$, we mark an accentuated movement at the level of the left fin by inclining the magnetic field $\gamma = 60°$ and $\gamma = 90°$.

For the case, a = 60°and γ = 0° the movement of the fluid becomes important at the intersection of the fluid fins, by increasing the inclination of the magnetic field the velocity of the ferrofluid becomes important at the bottom fin, which will be more important at γ = 90°, at this vertical position of the magnetic field and at the vertical of the fins a = 0° the ferrofluid is concentrated around the lower fin favoring the contact with the hot9 wall where the forced convection is improved to take its maximum Nuave = 5.4 Fig.10(a). The different orientations of the magnetic force give different effects of the Hartmann number that explain these behaviors. The thermal boundary layer has also increased as the angle of the magnetic field increases which is improved by increasing the fin inclination angle and therefore the heat transfer rate is improved.
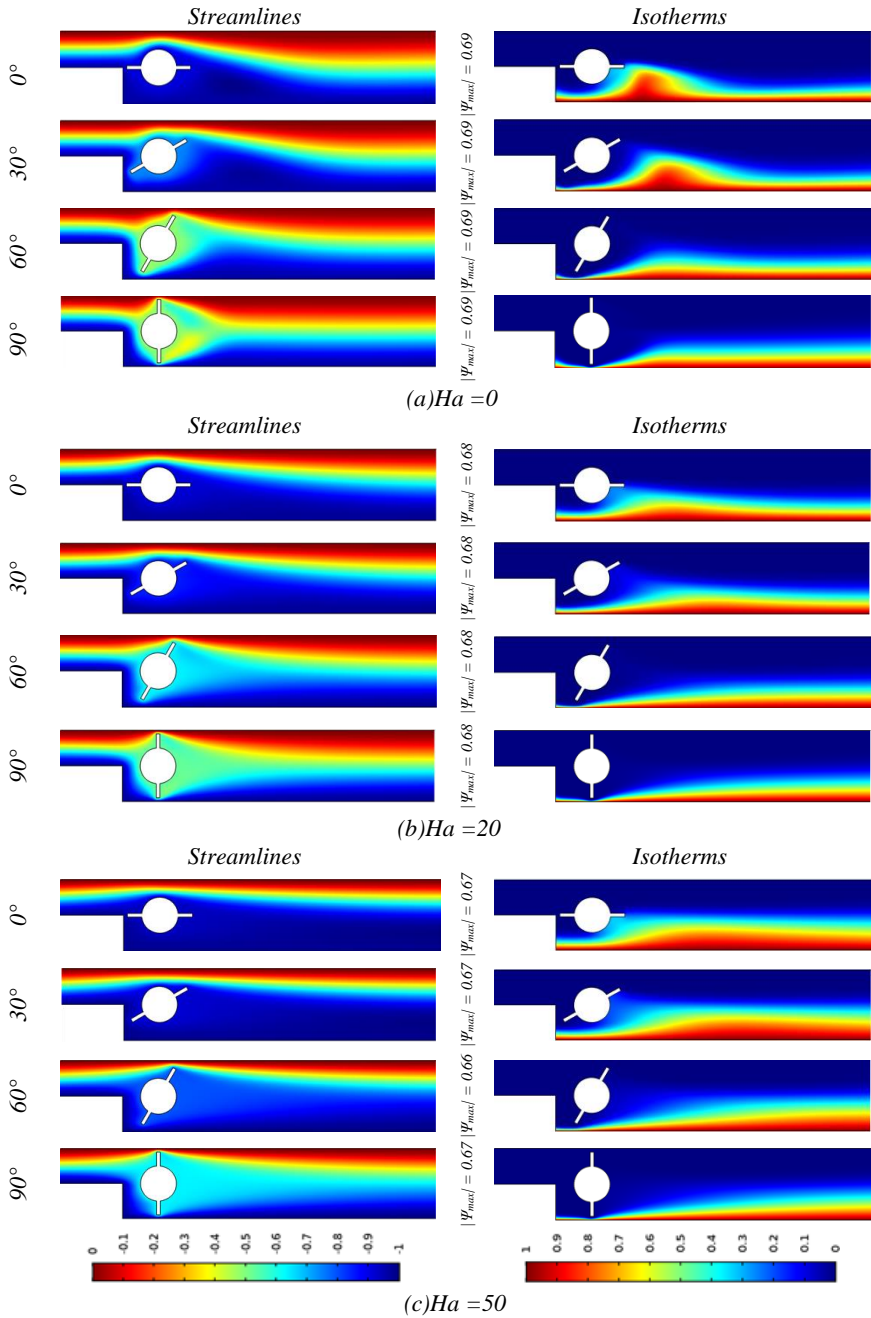
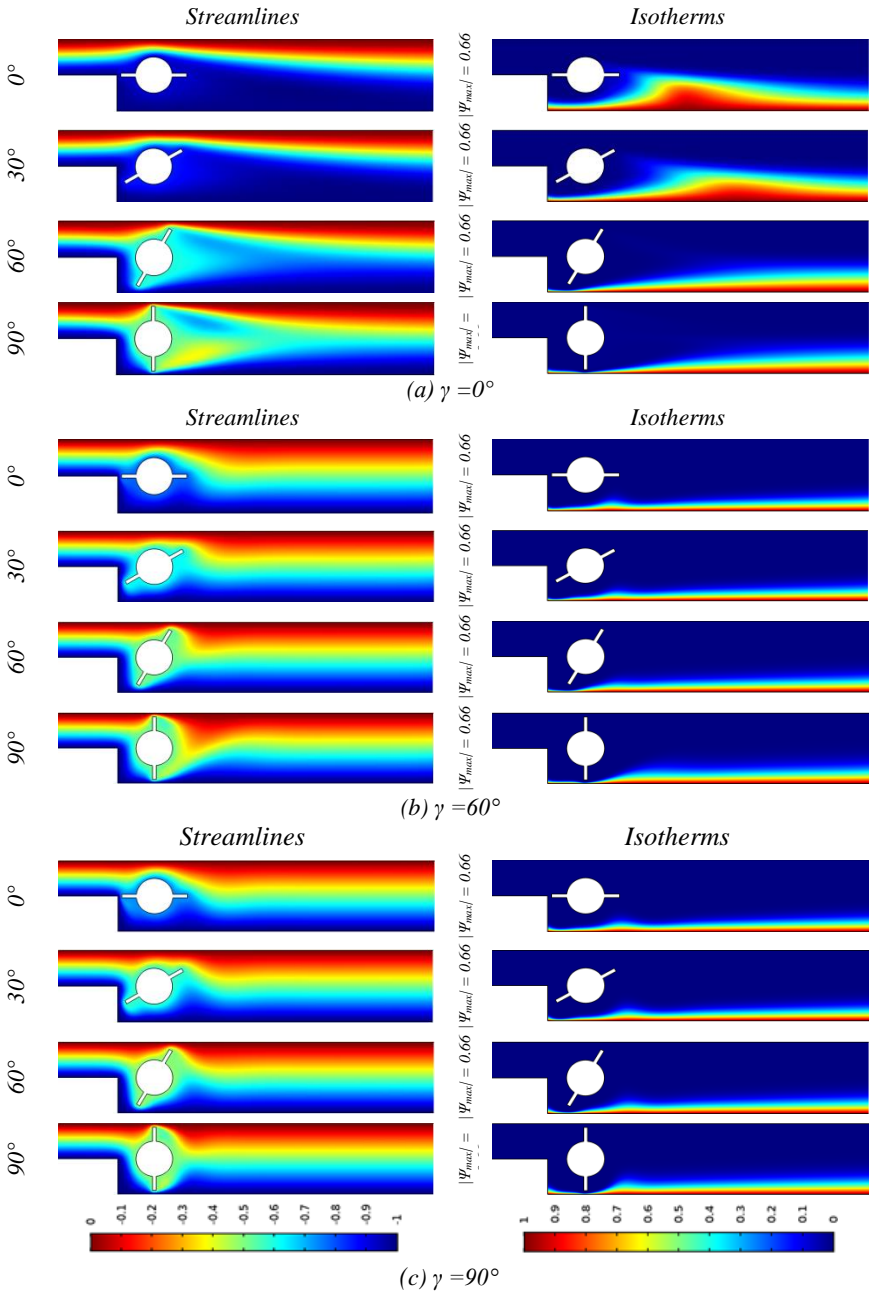*Fig. 3. Streamlines and isotherms for Ha = 0 (a), Ha = 20 (b), Ha = 50 (c), Pr = 6.2, Re = 50, γ = 0° and φ = 0.04.*

Fig. 4. Streamlines and isotherms for γ= 0° (a), γ = 50° (b), γ= 90° (c), Pr = 6.2, Re = 100, Ha = 0 and φ = 0. 04.

It was illustrated in Fig. 7 the contour of the streamlines and isotherms under the effects of Reynolds number variations: $Re = 10$, $Re = 100$ and $Re = 200$ at different angles of inclination of the fins: $a = (0°, 30°, 60°, 90°)$ for $Pr = 6.2$, $Ha = 20$, $\gamma = 0°$ et $\varphi = 4\%$. For the angle $a = 0°$, as well as a $=30°$ the Reynolds number increases, internal forces begin to dominate, so the flow becomes faster above the cylinder and slower below the cylinder at the fin- ferrofluid intersection. When we increase the Reynolds number at the position $a = 60°$ the flow accelerates at the intersection of the lower fin to mark in the position $a = 90°$ a concentration of Ferro-fluid in the case $Re = 200$ in addition an improvement of the thermal transfer. The increase of the Reynolds number generates an increase of the thermal layer, which improves in vertical position of the fins.

The streamlines and isotherms are presented in Fig. 8 by variations of the volume fraction of the ferrofluid: $\varphi = 0\%$, $\varphi = 4\%$, $\varphi = 10\%$ at different fin angle values: $a = (0°,30°,60°,90°)$ at fixed parameters: $Pr = 6.2$, $Re = 100$, $\gamma = 0°$, $Ha = 20$. At the position $a = 0°$ and $a = 30°$ with a fraction $\varphi = 0\%$, the fluid marks a weak flow in the bottom part, by increase the nanoparticle volume fraction the velocity of the flow increases at the level of the fins to achieve a maximum at the position $a = 90°$. In addition, we have a thermal layer that improves by increasing the volume fraction of ferrofluid as well as the angle of the fins that becomes important to the vertical position of the fins generating a good heat transfer, $Nu_{ave} = 5.8$ as observed in Fig. 10(b).

The effects of the Hartmann number Ha and the variation of the fin inclination angle on the Nu_{ave} number profiles for $Pr = 6.2$, $Re = 50$, $\varphi = 0.04$ are presented in Fig. 9(a). We consider a horizontal magnetic force $\gamma = 0°$. We notice a clear reduction in the Nu_{ave} number by increasing the Ha, and by inclining the fins the Nu_{ave} improves to reach a maximum at the position $a = 90°$. Physically, at the vertical of the fins, the magnetic force concentrates the ferrofluid flow at the bottom in contact with the hot wall, which causes an increase of the thermal boundary layer.

Profile's Nu_{ave} number for variations in Reynolds number Re at different fin inclinations at $Pr = 6.2$, $Ha = 20$, $\gamma = 0°$, and $\varphi = 0.04$ are given in Fig. 9(b). It should be noted that the Nu_{ave} is supported by increasing the Reynolds number and increasing the inclination of the fins where we note a $Nu_{ave} = 7.2$ at $a = 90°$ and Re $=200$. The increase of the Reynolds number at the vertical of the fins assures the good contact of the ferrofluid with the hot wall, which improves the convection.

Profiles of the Nu_{ave} for different values of magnetic field inclination angle *and at* $Pr = 6.2$, $Ha = 25$, $\gamma = 0°$ and $\varphi = 0$, are illustrated in Fig. 10 (a) at different fin angles. It can be seen that the Nu_{ave} increases with increasing magnetic field inclination and improves with increasing fin inclination, the maximum is at $\gamma = 90°$ at the vertical of the fins $a = 90°$. These behaviors are due to the fact that the inclination of the magnetic field gives different effects of the Hartmann number.
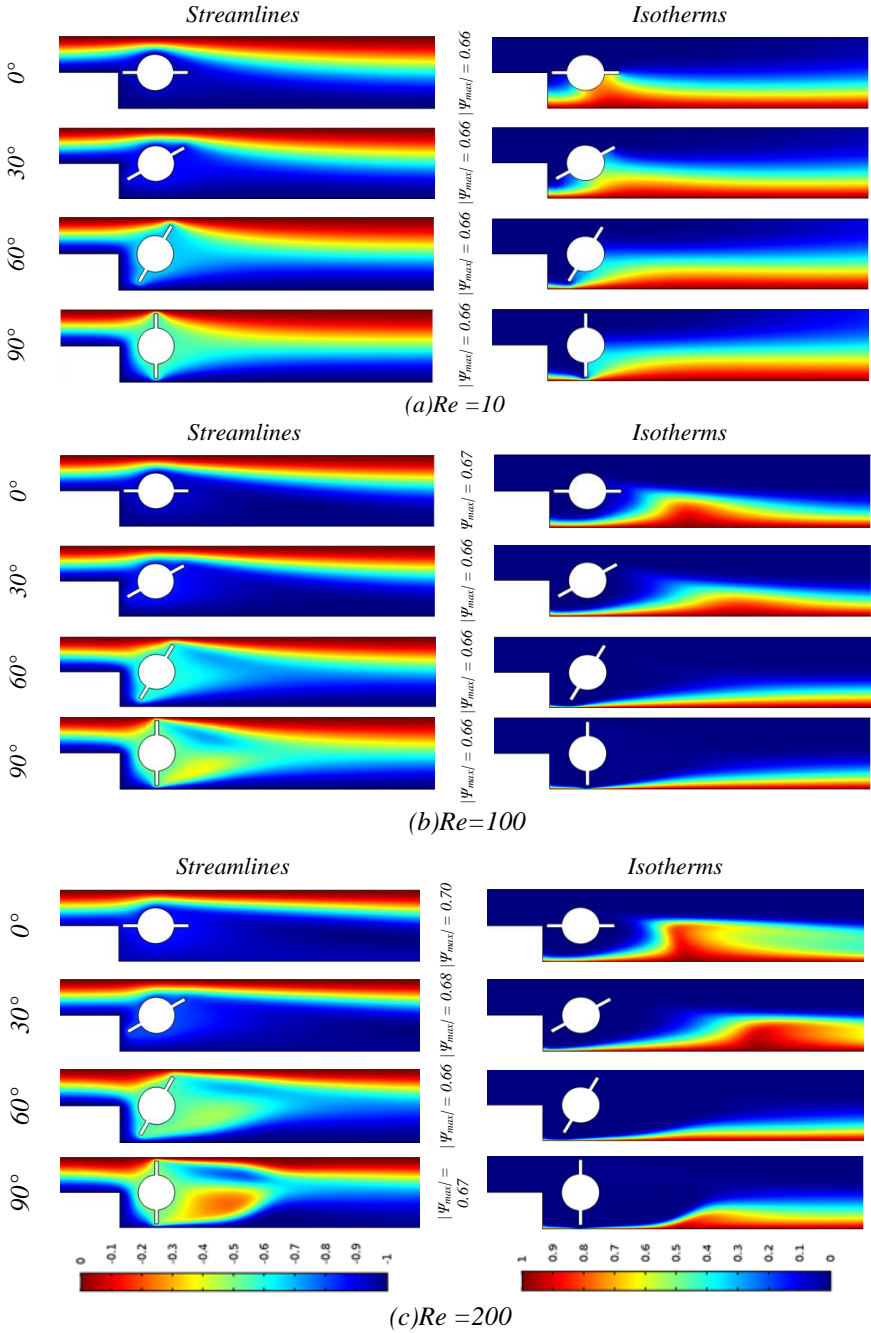
Fig. 5. Streamlines and isotherms for Re = 10 (a), Re = 100 (b), Re = 200 (c), Pr = 6.2, Ha = 20, γ = 0° and φ = 0.04.

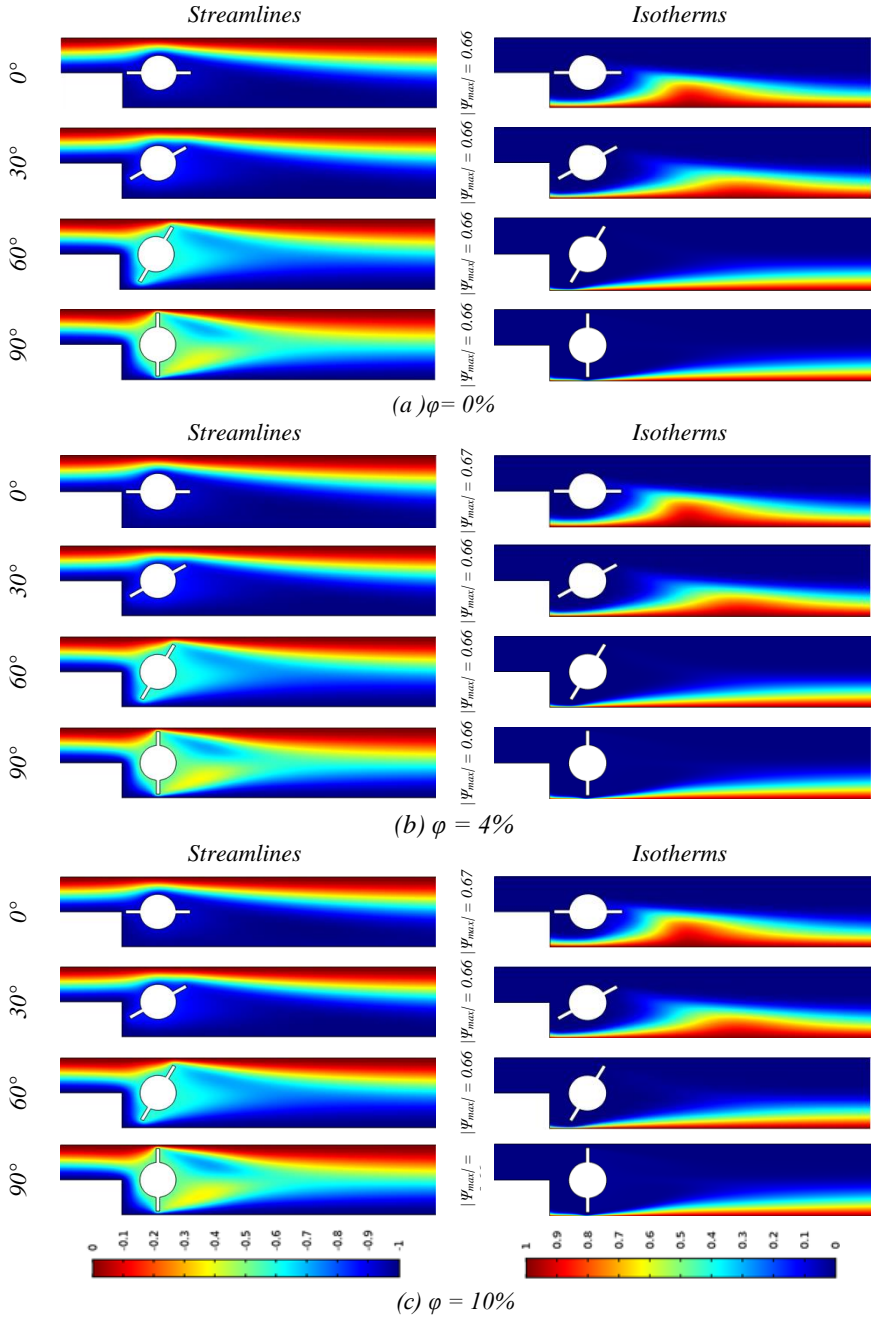*Fig. 6. Streamlines and isotherms for φ = 0 % (a), φ = 4%, (b), φ =10% (c), Pr = 6.2, Re = 100, Ha = 20, and γ = 0°.*

For different volume fractions of the ferrofluid and different inclinations at $Pr = 6.2$, $\gamma = 0°$, $Ha = 20$, $Re = 100$, profiles of the Nusselt average number are showed in Fig. 10(b). It is observed that the Nu_{ave} number increases progressively with the increase of the volume fraction as well as the angle of inclination, $Nu_{ave} = 5.8$ at $a = 90°$ and $\varphi = 0.1\%$. This is due to the thermal conductivity that increases as the volume fraction of the nanoparticles is concentrated at the bottom by the fin in a vertical position favoring the contact with the hot wall, which generates an improvement of the heat transfer rate.
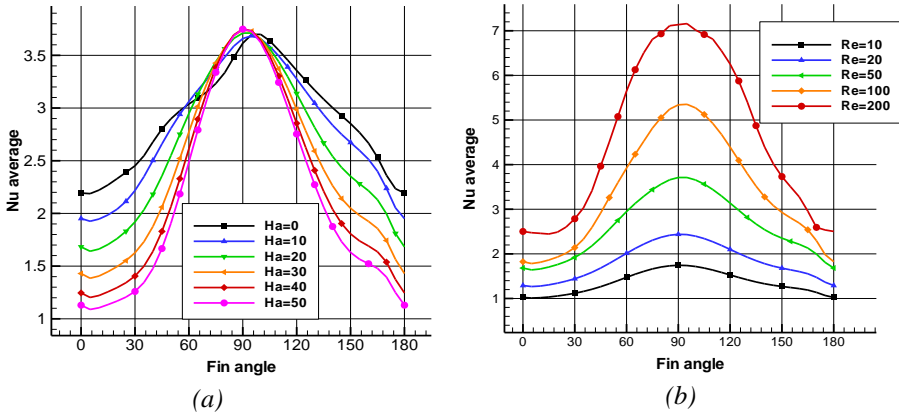
Fig. 7. Effect on Nu_{ave} at different fin angle (a) for Pr = 6.2 (a) of the Hartman number (Ha) at Re = 100, γ = 0° and φ = 0.04 (b) of the Reynolds number (Re) at Ha = 20, γ = 0° and φ = 0.04.

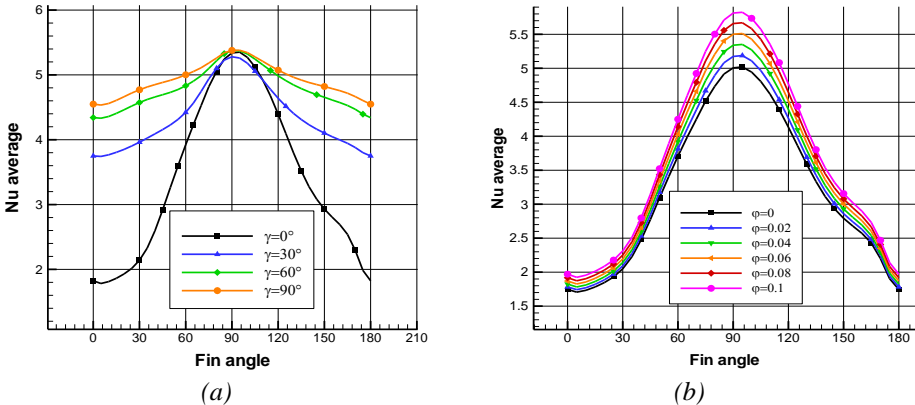*Fig. 8. Effect on Nu_{ave} at different fin angle (a) for Pr = 6.2 (a) of the magnetic field inclination (γ) at Ha = 20, Re = 100 and φ = 0.04 (b) of the nanoparticle volume fraction (φ) at γ = 0°, Ha = 20, Re = 100.*

Conclusion

In the present numerical study, the forced magnetohydrodynamic convection of the laminar flow of Fe_3O_4-H_2O inside a backward facing step geometry comprising a fixed cylinder with two fins has been studied. The finite element method has been used to solve the flow governing equations and wide ranges of governing parameters were considered. The following conclusions can be derived from the numerical simulation:

- The increase of the Hartmann number slows down the flow of ferrofluid, decreases the average Nusselt number, the vertical position of the fins makes the average Nusselt achieve a maximum value.
- The average Nusselt number increases as the angle of inclination of the magnetic field increases until it reaches a maximum value at a vertical angle of the fins.
- Variations in the volume fraction of the nanoparticles have positive effects on the average Nusselt number, which improves by inclining the fin angle to a maximum value at $a = 90°$.
- As the Reynolds number increases (inertial forces are supporting), the Nusselt number increases, inclining the fin angle to $a = 90°$ favors the transfer and the average Nusselt increases.

Nomenclature

Symbols

Cp	Specific heat [Jkg^{-1}K^{-1}]
K	Thermal conductivity [Wm^{-1}K^{-1}]
BFS	backward facing step
Ha	Hartmann number
q	heat flux density [Wm^{-2}]
Re	Reynolds number
Nu$_{ave}$	average Nusselt number
Nu	local Nusselt number
Pr	Prandtl number
P	Pressure [Pa]
x, y	Cartesian coordinates [m]
X,Y	Dimensionless coordinates
Re	Reynolds number
MHD	magnetohydrodynamic (MHD)
a	Fin angle[°]
T	Temperature [K]
v	Velocity component [ms^{-1}]

U, V	Dimensionless velocity component
$\bar{u}$	Vertical wall velocity [ms^{-1}]

Greek symbols

α	Thermal diffusivity [m^{2}s^{-1}]
β	Thermal expansion coefficient [K^{-1}]
θ	Dimensionless temperature
μ	Dynamic viscosity [kgm^{-1}s^{-1}]
ρ	Density [kgm^{-3}]
σ	Electrical conductivity [Ω^{-1}m^{-1}]
γ	magnetic field inclination angle
φ	Volume fraction

Subscripts

p	Nanoparticles
s	Solid
c	Cold
f	Base fluid
h	Hot
ff	Ferro-fluid

References

[1]   Ercan Erturk: Computers & Fluids, 37 (2008) 633-655.
[2]   H. Lan, B.F. Armaly, J. A. Drallmeier: International Journal of Heat and Mass Transfer, 52 (2009) 1690-1700.
[3]   Hiroshi Iwai, Kazuyoshi Nakabe, Kenjiro Suzuki: International Journal of Heat and Mass Transfer, 43 (2000) 457- 471.
[4]   Sabrina Star ("Kelbij"), Stabile Giovanni, Gianluigi Rozza, Joris Degroote: Applied Mathematical Modelling, 89 (2021) 486-503.
[5]   K. Kahine, V.T. Nguyen, M. Lebouché : Int. Comm. Heat Mass Transfer, Vol. 24, No. 8 (1977) pp.1103-1112.
[6]   Rashid Mahmood, Bilal S., Majeeda Afraz Hussain, Khan Ilyas, El-Sayed M.Sherif: j mater res technol, 9(2) (2020) 1978-1987.
[7]   A. Dejoan, M. A. Leschziner: International Journal of Heat and Fluid Flow, 25 (2004) 581-592.
[8]   Nicolas Benard, Patricia Sujar-Garrido, Jean-Paul Bonnet, Eric Moreaua: International Journal of Heat and Fluid Flow, 61(2016) 158-173.
[9]   Z.Y.Li, S.Guo, H.L.Bai, N.Gao: International Journal of Heat and Mass Transfer, 130 (2019) 240–251.
[10]   Yuki Koide, Ryota Sasaki, Yuki Kameya, Masahiro Motosuke: Experimental Thermal and Fluid Science, 66 (2015) 72-78.
[11]   J. Tihon, V. Pénkavová, M. Pantzali: European Journal of Mechanics B/Fluids, 29 (2010) 224-235.
[12]   Fatih Selimefendigil, F. Öztop Hakan: International Communications in Heat and Mass Transfer, 45 (2013) 111-121.
[13]   Kareem Ali Hilo, Abd Rahim Abu Talib, Acosta Antonio Iborra, Hameed Sultan Mohammed Thariq, Mohd Faisal Abdul Hamid: Powder Technology, 372 (2020) 497-505.
[14]   Hussein Togun , M. R. Safaei, Rad Sadri, S.N. Kazi, A. Badarudin, K. Hooman, E. Sadeghinezhad: Applied Mathematics and Computation, 239 (2014) 153-170.
[15]   E. Hamdi Ahmed, A.Sh. Kherbeet, M.I. Ahmed, B. H Salman: International Journal of Heat and Mass Transfer, 126 (2018) 963–973.
[16]   H. Abbassi, S. Ben Nassrallah: International Communications in Heat and Mass Transfer, 34 (2007) 231-237.
[17]   Ankit Kumar, K. Amit Dhiman: International Journal of Thermal Sciences, 52 (2012) 176-18 5.
[18]   Shafqat Hussain, E. Sameh Ahmed: Journal of Magnetism and Magnetic Materials, 484(2019).
[19]   A. Hussein Mohammed, F. Fathinia, B. Hari Vuthaluru, Liu Shaomin: Powder Technology, 346 (2019) 441-451.
[20]   A.Sh. Kherbeet, B.H. Salman, E. Hamdi Ahmed, A. Omer Alawi: International Journal of Heat and Mass Transfer, 79 (2014) 858-867.
[21]   Jizu Lv, Chengzhi Hu, Minli Bai, Liangyu Li Lin Shi, Gao Dongdong: Experimental Thermal and Fluid Science, 101 (2019) 151-159.
[22]   Ahmad Amiri, Hamed Arzani Khajeh, S. N. Kazi, B.T. Chew, A. Badarudin: International Journal of Heat and Mass Transfer 79 (2016) 538-546.
[23]   Martin Niemann, Jochen Fröhlich: International Journal of Heat and Mass Transfer, 101(2016)1237-1250.

[24] M. Atashafrooz: Journal of Thermal Analysis and Calorimetry (2019).

[25] M. Atashafrooza, M. Sheikholeslamib, H. Sajjadic: Journal of Magnetism and Magnetic Materials, 478 (2019) 216 –226.

[26] M. Atashafrooza, H. Sajjadib, Amiri A. Deloueic: International Communications in Heat and Mass Transfer, 110 (2020) 104411.

[27] M. Atashafrooz, H. Sajjadi, AmiriA. Deloueic, Tien-Fu Yang, Wei-Mon Yan: Numerical Heat Transfer, Part A: Applications (2021).

[28] M. Atashafrooz and S. A. Gandjalikhan Nassab S. A.: IJST, Transactions of Mechanical Engineering, Vol. 37 No. M1 (2013) 71-75.

[29] M. Atashafrooz, T. Asadi, Wei-Mon Yan: International Journal of Heat and Mass Transfer 156 (2020) 119837

[30] M. Atashafrooz: Journal of Thermal Analysis and Calorimetry (2019).

[31] M. Atashafrooz, S. A. Gandjalikhan Nassab, K. Lari: Heat Mass Transfer (2015).

[32] Meysam Atashafrooz, Seyyed Abdolreza Gandjalikhan Nassab, Khosro Lari: Journal of Mechanical Science and Technology, 29 (2) (2015) 845-859.

[33] Meysam Atashafrooz: Alexandria Engineering Journal, 57 (2018) 4277–4285.

[34] Protim Boruah Manash, R. Randive Pitambar, Pati Sukumar: International Journal of Heat and Mass Transfer, 125 (2018) 525-542.

[35] Fatih Selimefendigil, F. Öztop Hakan: International Communications in Heat and Mass Transfer, 45 (2013a) 111-121.

[36] Fatih Selimefendigil Fatih, F. Öztop Hakan: Computers & Fluids, 88 (2013b) 93– 107.

[37] Fatih Selimefendigil, F. Öztop Hakan: International Journal of Heat and Mass Transfer, 110 (2017) 231-247.

[38] Fatih Selimefendigil, F. Öztop Hakan: Advanced Powder Technology, 26 (2015) 1663-1675.

[39] Protim Boruah Manash, Pati Sukumar, R .Randive Pitambar: International Journal Heat and Mass Transfer, 137 (2019) 138-160.

[40] H. A. Mohammed, A. Alawi Omer, M. A. Wahid: Powder Technology, 275 (2015) 329-343.

[41] H.A Mohammed, A. N. Darus: Applied Mathematics and Computation, 240 (2014) 368-386.

[42] Abderrahim Mokhefi, Mohamed Bouanini, Mohammed Elmir: International Journal of Heat and Technology, Vol. 39, No. 1, February(2021) 251-261

[43] Abderrahim Mokhefi, Mohamed Bouanini, Mohammed Elmir, Pierre Spitéri: Metallurgical and Materials Engineering, (2021).

[44] Abderrahim Mokhefi, Mohamed Bouanini, Mohammed Elmir, Pierre Spitéri: Defect and Diffusion Forum SSN: 1662-9507, Vol. 409 (2021) 179-193.

[45] Abderrahim Mokhefi, Mohamed Bouanini, Mohammed Elmir, Yacine Guettaf: Chemical Papers, (2021).